OPEN ACCESS

GAVIN PUBLISHERS

Advances in Biochemistry and Biotechnology

Research Article

Tsubone TM, et al. Adv Biochem Biotechnol 5: 1098.
DOI: 10.29011/2574-7258.001098

In vitro Autophagy Modulation with Chloroquine: Some Lessons to Learn

Tayana Mazin Tsubone[1,4], Cleidiane de Sousa Rocha[1], Paulo Newton Tonolli[1], Watanabe II-Sei[2], Beatriz Simonsen Stolf[2], Maurício S. Baptista[1], Waleska Kerllen Martins[1,3*]

[1]Institute of Chemistry, University of Sao Paulo, São Paulo, Brazil

[2]Institute of Biomedical Sciences, University of Sao Paulo, São Paulo, Brazil

[3]Anhanguera University of Sao Paulo, São Paulo, Brazil

[4]Institute of Chemistry, Federal University of Uberlandia, Uberlândia - MG, Brazil

[*]**Corresponding author:** Waleska Kerllen Martins, Universidade Anhanguera de São Paulo, Avenida Professor Raimundo Pereira de Magalhães, 3.305. Pirituba, CEP 05145-200, São Paulo, Brazil

Citation: Tsubone TM, Rocha CS, Tonolli PN, II-Sei W, Stolf BS (2020) *In vitro* Autophagy Modulation with Chloroquine: Some Lessons to Learn. Adv Biochem Biotechnol 5: 1098. DOI: 10.29011/2574-7258.001098

Received Date: 21 January, 2020; **Accepted Date**: 04 February, 2020; **Published Date:** 10 February, 2020

Abstract

Objective: We attempt to investigate the mechanism triggered by Chloroquine (CQ) and its association with autophagic function.

Methods: To investigate the CQ effects on non-malignant and malignant cells, we performed cell viability assays, flow cytometry analysis, immunoblotting, immunofluorescence, confocal microscopy, electronic microscopy and Fluorescence Lifetime Imaging Microscopy (FLIM).

Results: The CQ harmful effects ended up higher in a long term-response (i.e., 48 h and 96 h after CQ-treatment during 24 h) compared to shorter ones (0 h or 24 h after CQ-treatment during 24 h). CQ provoked a lysosomal impairment intrinsically related to reduced proliferation and death in human carcinoma cells (HeLa, HT29, HepG2, and MCF7), as also melanomas SKMEL-25 and SKMEL-28. At long term-response, CQ induced cytotoxic effects on cells associated with the lysosomal accumulation and autophagy inhibition. Noteworthy, that other late effects in tumor cells included cellular nuclear abnormality, the beta-galactosidase senescent-associated activity, and increased lipofuscinogenesis, hallmarks of cell senescence. Remarkably, in the presence of the mitochondrially-toxic drug Oleanolic Acid (OA), a CQ lysosomal-mitochondrial axis of cellular stress could be modulated in tumor cells (HeLa, MCF7, and SKMEL-28), leading to autophagy-associated cell death.

Conclusion: CQ cytotoxicity is related to lysosomal impairment that leads to autophagy-associated cell death, nuclei abnormalities, lipofuscinogenesis, and senescence. Also, our findings indicate that a therapeutic approach based on lysosomal chemo-sensitization triggered by CQ parallel to mitochondrial OA-toxicity may represent a promisor strategy to overcome *in vivo* tumor progression relied on apoptosis lessening.

Keywords: Chloroquine; Autophagy; Cytotoxicity; Aging; Long-term response

Introduction

Considered a well-known example of repurposing success, Chloroquine (CQ) remains the drug of choice for malaria chemotherapy due to its substantial effectiveness [1-3]. Besides, CQ is an anti-inflammatory agent for the treatment of rheumatoid arthritis, lupus erythematosus, and amoebic hepatitis [2]. Preclinical evidence also revealed the efficacy of CQ in inhibiting the genesis and self-renewal of Cancer Stem Cells (CSC), underlining the potential of this "Old drug" as a repurposing strategy to open a new CSC-targeted chemoprevention era [4]. There are several examples of clinical trials employing CQ as an enhancing agent in cancer therapies (Table 1).

Cancer Type	Identifier	Study	Phase	Status	Ref.
Breast cancer	NCT01023477	CQ	I/II	1	[52]
	NCT02333890	CQ	II	2	-
	NCT01446016	CQ and taxane or taxane- like chemo agents	II	1	-
Brain	NCT01894633	Total-brain irradiation and CQ	II	1	-
	NCT02496741	CQ and metformin	Ib/II	1	[53]
	NCT01727531	CQ	-	1	-
	NCT03243461	CQ and temozolomide	III	3	-
	NCT00224978	CQ	III	1	[54,55]
	NCT02432417	CQ and chemoradiation	II	4	-
	NCT02378532	CQ and chemoradiation	I	1	-
Melanoma	NCT01469455	DT01 with radiotherapy and CQ	I	1	-
	NCT03979651	Trametinib plus hydroxychloroquine in patients with metastatic neuroblastoma RAS melanoma		4	-
Multiple myelomas	NCT01438177	CQ, velcade, and cyclophosphamide	II	1	[56]
Pancreatic	NCT01777477	CQ and gemcitabine	I	1	-
Prolactinoma	NCT03400865	Cabergoline and hydroxychloroquine/CQ	-	4	-
Small cell lung cancer	NCT00969306	CQ and A-CQ 100	I	1	-
	NCT01575782	CQ	I	1	-
Solid tumors	NCT02071537	CQ and carboplatin/gemcitabine	I	1	-
1 Completed or terminated; 2 Unknown; 3 Recruiting; 4 Not yet recruiting. Source: ClinicalTrials.gov [http:// https://clinicaltrials.gov/]					

Table 1: Clinical trials of the CQ effects on human cancers.

Considering that cancer cells might use autophagy as a pro-survival mechanism to deal with unfavorable conditions, increasing their growth and aggressiveness [5,6], CQ and its analogs would be promising antitumoral drugs [2,4]. CQ seems to exert its biological effects through a weak base lysosomotropic feature. In its unprotonated form, CQ can diffuse across lysosomal membranes to become protonated and accumulate in these acidic organelles [2]. Once trapped within lysosomes, CQ raises intra lysosomal pH and interferes with autophagosome-lysosome fusion events [7]. This unique property has established CQ as the most widely used drug to sensitize cancer cells through inhibiting autophagy *in vitro* and *in vivo* [2,6]. Although it is well-known that autophagy, a lysosome-dependent degradation pathway, participates in critical cellular functions including homeostasis and energy production [8], differentiation [9], and aging [10-12], the molecular events that trigger the loss in autophagy-lysosomal homeostatic axis are still object of conjecture [7]. To further improve the directions of research on CQ- mediated cancer control, we need to understand how the anti-autophagic effects of CQ function in the context of cellular and molecular control pathways in cells. In this context, we studied the harmful effects of CQ on autophagy in a long-lived post-challenged cell. Aiming to avoid artifacts that may occur when employing transfection and transgenesis strategies to monitor endogenous LC3 lipidated form (LC3B-II) [13], we used nonmalignant immortalized human keratinocytes (HaCaT) as a cellular model, in which autophagy plays a homeostatic role in keratinocyte differentiation [9]. For our knowledge, this study is the first to investigate further the adverse CQ effects on autophagy through a time-point analysis. To perform a comparative analysis regarding tumor histologic type, we also evaluated the CQ effects on human carcinoma and melanomas cells.

This study also showed for the first time the long-term cytotoxicity of CQ as an aging-senescent agent on human tumor cells and nonmalignant HaCaT cells that require autophagy for maintenance of homeostasis. Indeed, by assessing cellular outcome in the long-term analysis, we showed that CQ triggers autophagy associated with cell death, aging, and senescence linked to a lysosomal- mitochondrial axis of cellular stress [14,15]. Also, our findings indicate a new therapeutic approach based on lysosomal chemo-sensitization triggered by CQ parallel to mitochondrial toxicity by the pentacyclic triterpenoid Oleanolic Acid (OA), which may represent a promisor strategy to overcome tumor resistance.

Methods

Cell lines and cell culture

Prof. Hugo Armelin (Instituto Butantan, Sao Paulo, Brazil) supplied HaCaT [16], and the human tumor cells HeLa, HT29, HepG2, MCF7, SKMEL-25, and SKMEL- 28 were gently provided by Ludwig Institute for Cancer Research, Sao Paulo, Brazil. HaCaT, HeLa, HepG2 and SKMEL-25/28 cells were cultured in Dulbecco's Modified Eagle Medium (DMEM, Gibco™, 12100046) supplemented with 10% (v/v) Fetal Bovine Serum (FBS, Gibco™, 12657029), 100 units/mL of penicillin, 100 µg/mL of streptomycin and 250 ng/mL of amphotericin B and incubated at 37 ˚C under a humidified atmosphere of 5% carbon dioxide [16-18]. MCF7 cells were cultured in DMEM /F-12 without phenol red (Gibco™, 21041025) and HT29 cells in Minimum Essential Medium (MEM, Gibco™, 61100061). All cell lines were used up to 25 passages after thawing. A curve of cell density previously determined the ideal cell confluence in the function of incubation time (data not shown). Then, for all times of evaluation (24 h, 48 h, or 96 h after CQ treatment for 24 h), experiments were performed in culture dishes (96 well TC-treated polystyrene microplate, Corning®, 3599) with non-confluent cells.

Chloroquine (CQ) treatment

A stock solution of CQ (Chloroquine diphosphate salt, Sigma, C6628) was prepared at 20 mM in Milli-Q H_2O, sterilized by filtration 0.2 µm and stored in aliquots at -20 ˚C until use. The appropriate amounts of stock solutions were diluted in DMEM with 1.0% (v/v) FBS to prepare work solutions; we treated cells with CQ in a dose-dependent manner (0 to 100 µM). Non-treated cells in DMEM 1.0% (v/v) FBS served as control (CT). After 24 h of incubation with CQ, cells were washed in Phosphate-Buffered Saline (PBS, potassium phosphate monobasic 1.76 mM, sodium chloride 137 mM, potassium chloride 2.7 mM, sodium phosphate dibasic 10 mM, pH 7.2) and further incubated in DMEM 10% (v/v) FBS supplemented with antibiotics and fungicide for 0 h (i.e., T1), 24 h (i.e., T2), 48 h (i.e., T3) and 96 h (i.e., T4).

Cell survival assays - MTT and CVS

We performed independent CVS (Crystal Violet Staining) and MTT assays as described [13]. Briefly, at T3, we washed cells and added medium with 1% (v/v) FBS containing Methylthiazolyldiphenyl-tetrazolium bromide (MTT, Sigma-Aldrich, M5655) at 50 µg/mL and incubated for 2 h in a humidified atmosphere containing 5% CO_2 at 37 ˚C. Next, we solubilized the reduced-product formazan in 0.2 mL DMSO (Synth, Brazil), and read absorbance values at 550 nm with a wavelength correction set at 800 nm for the subtraction of backgrounds, using the Infinite M-200 Tecan microplate reader (Männedorf, Switzerland). For the CVS assay, NR-fixed cells (see below) were stained with crystal violet (CV, Sigma- Aldrich, C6158) at 0.02% (w/v) for 5 min at room temperature. Next, we recorded the absorbance of eluted CV with 0.1 M sodium citrate in 50% (v/v) ethanol at 585 nm [13]. We normalized cell survival rates to the absorbance values of untreated cells.

AAU calculation

The nonfunctional autolysosomes accumulate in cells leading to autophagy- associated cell death [15,19,20]. To assess this effect, after CQ-treatment, we determined the numeric variable AAU (autophagy arbitrary units) for each condition [13]. Briefly, at T3 cells were incubated with 30 µg/mL neutral red (NR, Sigma-Aldrich, N4638) for 2 h at 37 ˚C incubator under a humidified atmosphere at 5% carbon dioxide. Next, we eluted NR with an alcoholic-based 1% (v/v) acetic acid fixing solution and measured its absorbance at 540 nm as described above. These fixed cells were washed with water and used for CVS assay (above).

Finally, to calculate AAU (1), the mean NRU survival rate was normalized to the mean of the MTT and CVS survival rates according to the function w (x, y, z):

$$w = \frac{1}{2}\left[\left(\frac{x}{y}\right) + \left(\frac{x}{z}\right)\right] \qquad (1)$$

Where x, y, and z were the survival rates measured by NRU, CVS, and MTT assays, respectively [15].

Acridine Orange (AO) staining of live cells

For AO live-cell imaging experiments, we stained cells according to published procedures [13,21]. Briefly, the lysosomotropic dye AO (Acridine Orange hemi (zinc chloride) salt, Sigma, A6014) was added to a final concentration of 1.0 µg/mL for 10 minutes at 37 ˚C in a humidified CO_2 incubator. After washing twice in PBS, live-cells were visualized using a microscope (Zeiss™ Axiovert 200, Germany) equipped with an inverted microscope for transmitted light and epifluorescence (Zeiss™ Axiovert 200, Germany) equipped with a C-APOCHROMAT 40X/1.20 W Corr M27 objective (Zeiss™, 421767-9970-000) and imaged using Image J Software (National Institutes of Health, Bethesda). Dye fluorescence was detected using the filter set 09 (Zeiss™, 488009-9901-000) that provides an excitation bandpass (BP) of 450 to 490 nm with emission Long Pass (LP) of 515 nm.

Staining and flow cytometry analysis of lysosomes with AO

AO is a lysosomotropic weak base (pKa = 10.3) that is retained (in the protonated AOH^+ form) due to proton trapping in lysosomes (pH 4.5-5.5). Under excitation with blue light (λ = 488 nm), AO dimers (formed under high AO concentration) exhibit red fluorescence, while AO monomers (low AO concentration) show green fluorescence [22]. The end-stage of lysosomal damage may be evaluated by the AO uptake method, as previously described [23]. Immediately after treatment with CQ (60 µM) for 90 min, HaCaT was incubated with AO (10 µg/mL) for 15 min in a standard culture medium at 37 ˚C, such that AO accumulated in stable lysosomes. Then we rinsed cells with culture medium in the dark and incubated under standard culture conditions for another 10 min to reduce cytosolic AO. Next, after washing twice in PBS, we collected at least 20,000 events for flow cytofluorometric analysis of AO (FL1 and FL3) using BD FACS Verse™ and FlowJo software. Since AO only accumulates in stable lysosomes, we assessed the extent of lysosomal impairment by comparing the amount of red and green fluorescence.

Immunoassays and confocal microscopy

Supernatant cells were washed out, and adherent cells were immunoassay after fixation in 4% (w/v) formaldehyde in PBS pH 7.4, washing, blocking and incubation with primary monoclonal antibodies against cytochrome c oxidase complex IV (COXIV, Molecular Probes, A21347), cathepsin B (CTSB, [CA10], Abcam®, ab58802), lysosome-associated membrane protein 2 (LAMP2A, [H4B4], Abcam®, ab25631), LC3B (D11 XP®, Cell Signaling Technology®, 3868) and SQSTM1/p62 ([D10E10], Cell Signaling Technology®, 7695), according to manufacturer's instructions. Then we incubated cells with goat Alexa Fluor-coupled antibodies against rabbit IgG (H+L) (A-11034 and A-21070) or mouse IgG (A-11001 and A-21050, Molecular Probes). We analyzed the DAPI-counterstained slides using a confocal microscope (Zeiss™ Axiovert 200 LSM 510 Laser, Carl Zeiss, Germany) equipped with a Plan-APOCHROMAT 63X/1.40 oil DIC M27 objective (Zeiss™, Carl Zeiss, Germany) and determined the overlap between these proteins as described previously [24]. LysoTracker™ Red DND-99 (LTR, L7528) is an acidophilic probe compatible with aldehyde fixation and thus may be combined with the immunofluorescence detection of proteins such as COXIV, CTSB, LC3B-II and SQSTM1 [20].

We analyzed the slides using filter sets that provide an excitation of 364, 488, 543 and 633 nm with emission bandpass (BP) of 437 to 490 nm, 515 to 534 nm, 565 to 640 nm and 651 to 704 nm to detect the fluorescence of DAPI, Alexa Fluor® 488, LTR and Alexa Fluor® 633, respectively.

Analysis of mitochondrial transmembrane potential (ΔΨm)

We used the probe MitoTracker™ orange CMTMRos (MTO) to monitor mitochondrial inner transmembrane potential (ΔΨm). After washing, MCF7 cells were incubated with MTO (50 nM) in 1% (v/v) FBS DMEM for 30 min in a 37 ˚C incubator with a moist atmosphere of 5%carbon dioxide. Following treatmentwith DMSO or OA (20 µM) for 3 h, we washed cells and performed fixation with cooled 4% (w/v) formaldehyde pH 7.2 in PBS. After washing, slides were mounted in ProLong™ gold antifade reagent containing DAPI nuclear stain. We used filter sets that provide excitation of 364 and 543 with emission BP of 437-490 nm and 554- 608 nm to detect the fluorescence of DAPI and MTO, respectively.

Measurement of cathepsin activities

We treated HaCaT with CQ (60 µM) for 24 h and evaluated the cathepsin activity at T3 by a fluorimetric assay (K140-100 and K142-100, Bio Vision Inc.). Briefly, HaCaT cells were lysed in 50 to 100 µL of chilled lysis buffer and incubated on ice for 10 min. After collection cytosolic fraction, we obtained whole-cell extracts after lysing the cell debris above with more 50 to 100 µL of chilled lysis buffer followed by freeze/thaw cycles (3 x). Next, we centrifuged at 10,000 g for 10 min at 4 ˚C these whole-cell lysates. We measured the protein concentration in the same aliquot using the BRADFORD assay (Bio-Rad Laboratories, Hercules, CA, USA), and we applied 15 µg of protein per sample for enzymatic assays. Enzyme activity was expressed in arbitrary units (a.u.) as a ratio to control.

Nuclear Morphometric Analysis

To perform Nuclear Morphometric Analysis (NMA) of cells treated with CQ (60 µM) at T3, we stained nuclei with DAPI and captured images under an inverted fluorescent microscope (Zeiss™ Axiovert 200 LSM 510 Laser, Carl Zeiss, Jena, Germany). By using Image J Software´s NII Plugin, we evaluated parameters of nuclear size and shape for a large number of cells [15,25]. The parameters considered were Aspect (Asp), Area box (Arbx), Radius ratio (Rr), and Roundness (Rou), which were combined in an index called Nuclear Irregularity Index [NII = Asp - Arbx + Rr - Rou] [25].

Transmission Electron Microscopy (TEM)

At T3 after treatment with CQ (60 µM), lipofuscin-loaded cells were collected and fixed for 8 h at 4 ˚C in modified Karnovsky's solution, 2.5% (v/v) glutaraldehyde and 2% (v/v) formalin in 0.1 M sodium phosphate buffer, pH 7.4. Also, we performed a post-fixation with 1% (v/v) osmium tetroxide solution for 2 h at 4 ˚C. After dehydration in several graded ethanol baths 70 to 100% (v/v) and propylene oxide, we embedded cells in synthetic resin [26]. Cell sections (90 nm) were obtained using a Reichert Ultracut E microtome and mounted on Formvar films (200 mesh). We analyzed under transmission electron microscopy (Jeol 1010 80KV, Tokyo, Japan) ultrathin samples, after counterstaining with uranyl acetate and lead citrate.

Detection of lipofuscin granules

Were washed with PBS HaCaT cells incubated with CQ (60 µM) for 24 h and chased them further for 48 h in the presence of DMEM 10% (v/v) FBS. After the second washing in PBS and fixing with 4% (w/v) formaldehyde in PBS pH 7.4, we rewashed coverslips and mounted them in ProLong® diamond antifade reagent without DAPI nuclear stain (Molecular Probes®, P36961). Slides were analyzed under a fluorescence confocal microscope (Olympus IX 73) FluoView FV1000 with a piezo-driven objective scanning coupled to the MicroTime 200 system (PicoQuant-Berlin, Germany) for detection of fluorescence lifetime. To detect lipofuscin granules, we used a filter set that provides excitation at 509 nm with a long emission pass at 519 nm. Time decays were fitted using SymphoTime 64 (version 2.1) and TimeHarp platform, which transformed single-photon-counting decays in FLIM images.

Senescence-associated β-galactosidase activity

The replicative senescence was evaluated by the SA-βgal assay, as described before [27]. After a 24 h-treatment with CQ (60 µM), the HaCaT cells were washed and refreshed with DMEM (Sigma-Aldrich) supplemented with 10% (v/v) FBS, 100 units/mL of penicillin, 100 µg/mL of streptomycin and 250 ng/mL of amphotericin B. 96 hours the 24 h-treatment with CQ cells were fixed with methanol and visualized using an inverted microscope for transmitted light (Zeiss™ Axiovert 200, Germany).

Statistics

Statistical analysis was performed using IBM® SPSS Statistics version 20. We calculated the strength of linear correlation analysis by the Spearman´s coefficient (rho). Statistical analysis was employed to compare groups of samples by one-way analysis of variance (ANOVA) with Dunnett T3 or Bonferroni post-hoc tests, depending on the homogeneity of variance. We analyzed data obtained from at least three independent experiments and expressed the results as mean values ± standard error. P values lower than 0.05 were considered statistically significant.

Results

The main experimental procedure employed in this work consisted of incubating HaCaT or human tumor cells HeLa, HT29, HepG2, MCF7, SKMEL-25, and SKMEL-28 with CQ. We reported the results referring to the time at which we experimented with the incubation with compounds. We used the label T1, T2, T3, and T4 referred to experiments performed 0, 24, 48, and 96 hours after a 24 h incubation period with CQ.

CQ toxicity dependent on a long-term response

Several reports have shown the CQ cytotoxic effects on mammalian cells by triggering autophagy-associated cell death, mainly in tumors cell lines [6,28-30]. Pronounced *in vitro* inhibition of cancer cell growth (reaching 50% inhibition) was reported using CQ at doses from 64 µM to 935 µM in a short-term response (see Table 2).

Cell line	IC50 (µM) with CQ-treatment during 24 h	Time of evaluation after CQ treatment	Ref.
MCF7	480	---	[57]
T-47D	735	---	[57]
HeLa	650	---	[57]
Caco-2	490	---	[57]
HCT116	884	---	[57]
HEp-2	555	---	[57]
HepG2	935	---	[57]
PC3	905	---	[57]
CT26	100	2.5 h	[58]
A549	128	---	[59]
4T1	100	0 h	[60]
Bcap-37	64	0 h	[60]
A549	120	4 h	[61]
H460	100	4 h	[61]
5637	100	14 days	[62]
T24	100	14 days	[62]
PANC-1	500	3 h	[63]
BxPC-3	500	3 h	[63]
ARPE-19	250	4 h	[64]
NCHI-H460	137.5	3 h	[65]

Table 2: IC50 values and time evaluated after CQ-treatment in several human malignant cell lines.

Although reports have focused on chloroquine as a repurposing "Old drug" in cancer treatment [31], we hypothesized that CQ might also be dependent on-time response. Then, we investigated long-term response on cells that originate from epithelium, such as HaCaT [16], HeLa, and MCF7.

To determine the survival rate in long-term cytotoxicity, we allowed HaCaT to proliferate for almost two doubling times after CQ-treatment (i.e., 48 h). By varying CQ concentrations from 0 to 100 µM, we found that there was a negligible cell death with 20 to 40 µM of CQ. However, HaCaT cell viability significantly decreased upon CQ at 60 µM (42.0 ± 0.5%) or 100 µM (18.6 ± 0.5%) (Figure 1A). Note that the remarkable decrease in cell survival determined by MTT and CVS assays occurred upon CQ concentrations below those IC50 values reported for different cancer cells (see Table 2).

The biological CQ effect on HaCaT was closely associated with the status of autophagy inhibition related to lysosomal impairment and accumulation [13]. Lysosomal accumulation in terms of levels (AAU) [13] significantly augmented as CQ concentration increased, rho = -0.85 ($p<0.00001$) (Figure 1B). Staining with the lysosomotropic base dye Acridine Orange (AO) revealed at T1 a conspicuous vacuolization in fusiform, living CQ-treated cells compared to the epithelioid non-treated cells (Figure 1C). Moreover, microscopy images showed that this vacuolization increased in a time-dependent manner. Comparing T3 to T1, we noted a pronounced enhancement of vacuolization in CQ-treated cells that associated with a remarkable increase of the nuclei size (Figure 1C).

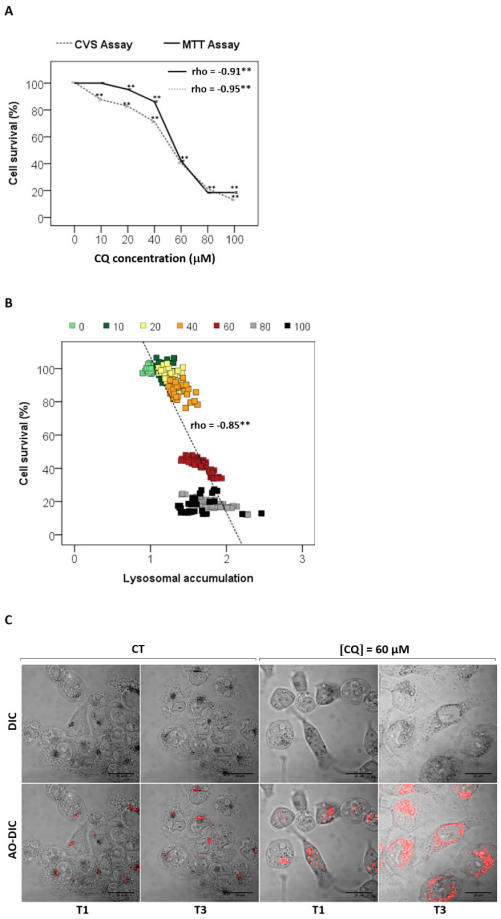

Figure 1: CQ effects on HaCaT evaluated in a time-dependent manner. (**A**) T3 after treatment with CQ (0 to 100 µM), we determined by CVS and MTT assays HaCaT cell survival rates (%). (**B**) A linear correlation between lysosomal accumulation and cellular survival (%) measured by linear Spearman´s coefficient (rho) in the function of CQ concentration. (**C**) Differential Interference Contrast (DIC) microscopy images of HaCaT treated with CQ (60 µM) stained with Acridine Orange (AO) after indicative times. T1 = 0 h; T2 = 24 h; T3 = 48 h and T4 = 96 h after incubation with CQ during 24 h. We obtained all results from at least three independent experiments and expressed as mean values ± standard error. We indicated the significance levels as $^{*}p<0.05$, $^{**}p<0.00001$. Scale bars: 20 µm.

CQ toxicity at long-term response is associated with autophagy inhibition

To evaluate CQ effects on lysosome stability, we analyzed the release of proton trapped AO by flow cytometry (Figure 2A). A significant increase of green cytoplasmic fluorescence was observed in CQ-treated HaCaT cells after incubation for 90 min in comparison to control, p=0.021 (Figure 2A). This result suggests that AO fails to accumulate in a subset of lysosomes since CQ dissipates the proton gradient by exerting a proton sponge effect [22]. We observed that CQ (60 µM) decreased the sequestration of LysoTracker™ Red DND-99 (LTR) in lysosomes 3.5-fold (p=0.033) compared to control (Figure 2B), probably because of lysosomal impairment by raising pH [32].

A well-known indication of damage in lysosomes is the redistribution of cathepsin B (CTSB) from a punctate lysosomotropic pattern to a diffuse cytoplasmic localization (in a) because of lysosomal membrane permeabilization [21,33]. When CTSB release was monitored by indirect immunofluorescence using an automated confocal imaging approach, we found a subcellular redistribution of lysosomal CTSB into discrete cytoplasmic dots (in b) that markedly increased 6 h after treatment with CQ (60 µM) compared to control cells (Figure 2C). This subcellular redistribution of endogenous CTSB into bulk cytoplasmic dots (green) was closely associated with lysosomal instability by the absence of LTR uptake after CQ-treatment (Figure 2C).

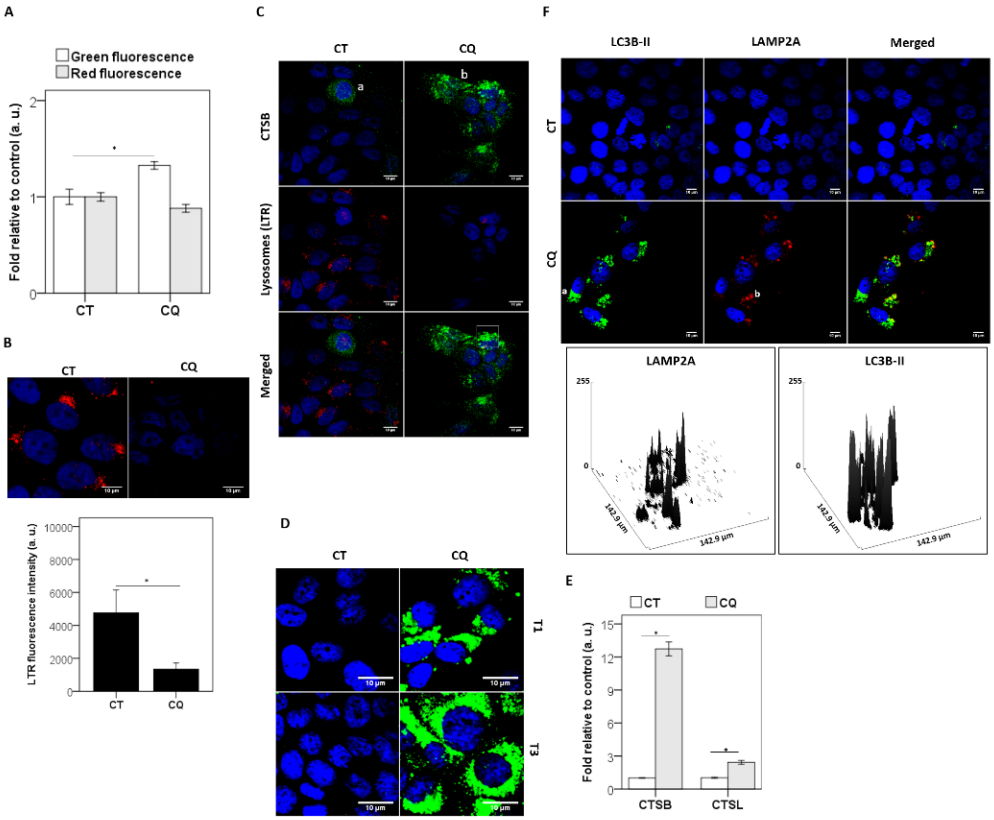

Figure 2: The CQ effects on HaCaT connected to autophagy inhibition. **(A)** Green and red fluorescence of AO were expressed as arbitrary units (a. u.) after ratio to control in HaCaT treated with CQ (60 µM) for 90 min. **(B)** Fluorescence images of HaCaT treated with CQ (60 µM) and stained with LysoTracker™ red DND-99 (LTR) 6 h after treatment. **(C)** HaCaT stained with LTR (red) and immunoassay for cathepsin B (CTSB) in green within 6 h after CQ (60 µM) treatment. **(D)** Immunofluorescence images of LC3B-II in HaCaT at T1 and T3 following treatment with CQ (60 µM). **(E)** At T3 lysosomal enzymes were extracted from lysosomal fraction, following fluorescence assays for detection of cathepsins L (CTSL) and B (CTSB) activities. Bars represent arbitrary units (a. u.) after ratio to control in HaCaT treated with CQ (60 µM). **(F)** Co-localization images of a lysosomal marker LAMP2A (red) and the autophagosome marker LC3B-II (green) in HaCaT at T2 following treatment with CQ (60 µM). Surface plots show the fluorescence intensity of LC3B-II and LAMP2A.T1 = 0 h and T3 = 48 h after incubation with CQ. We obtained all results from at least three independent experiments and expressed as mean values ± standard error. We indicated the significance levels as $^{*}p<0.05$, $^{**}p<0.00001$. Scale bars: 10 µm.

To confirm if lysosomal instability caused by CQ was related to autophagy inhibition, we compared the abundance of LC3B-II, a well-recognized hallmark of autophagy, which reflects the recruitment of LC3B-lipidated form to phagophores and their maturation to autophagosomes [19]. As expected, immunofluorescence microscopy analysis revealed that CQ (60 µM) induced a significant accumulation of LC3B-II, a known pattern of inhibition of autophagic flux [20,34,35]. The more pronounced LC3B-II expression at T3 compared to T1 indicates that the autophagic flux inhibition occurs in a time-dependent frame (Figure 2D). Note that as autophagy inhibition persisted (as stated by LC3B-II accumulation), there was a remarkable increase in nuclei size at T3 compared to T1. Interestingly, these biological effects were observed even upon recruitment of lysosomal proteases (e.g., CTSB and CTSL) with activities significantly increased in CQ-treated cells compared to control ($p<0.00001$) (Figure 2E). Interestingly, these biological effects were observed even upon recruitment of lysosomal proteases(e.g.,CTSB and CTSL) with activities significantly increased in CQ-treated cells compared to control ($p<0.00001$) (Figure 2E).

Next, we evaluated the status of LC3B-II degradation and its co-localization with lysosome marker LAMP2A in CQ-treated and non-treated HaCaT cells at T2 (Figure 2F). The co-localization of the lysosomal marker and LC3B-II illustrated by confocal micrographs endorsed a remarkable accumulation of autophagosomes (a) and autolysosomes (b) after CQ-treatment (Figure 2F).

Altogether, our data indicate that CQ induces autophagy inhibition in nonmalignant cells in a time-dependent frame, resulting in Regulated Cell Death (RCD) [36]. Also, we observed the same extension of CQ regarding autophagy status on malignant cells. By chasing treated cells at T2, a remarkable accumulation of autolysosomes was observed in HeLa cells by co-staining lysosomes (LTR), cathepsin B (CTSB), and SQSTM1/p62, a biomarker of selective autophagy [19] (Figure 3A). The induction of selective autophagy (e.g., mitophagy) [37] was confirmed by double-immunoassaying for SQSTM1 and the mitochondrial biomarker COXIV (Figure 3B). The amount of damaged or worn-out mitochondria substantially increased in CQ-treated cells compared to control, an increment correlated to the accumulation of SQSTM1.

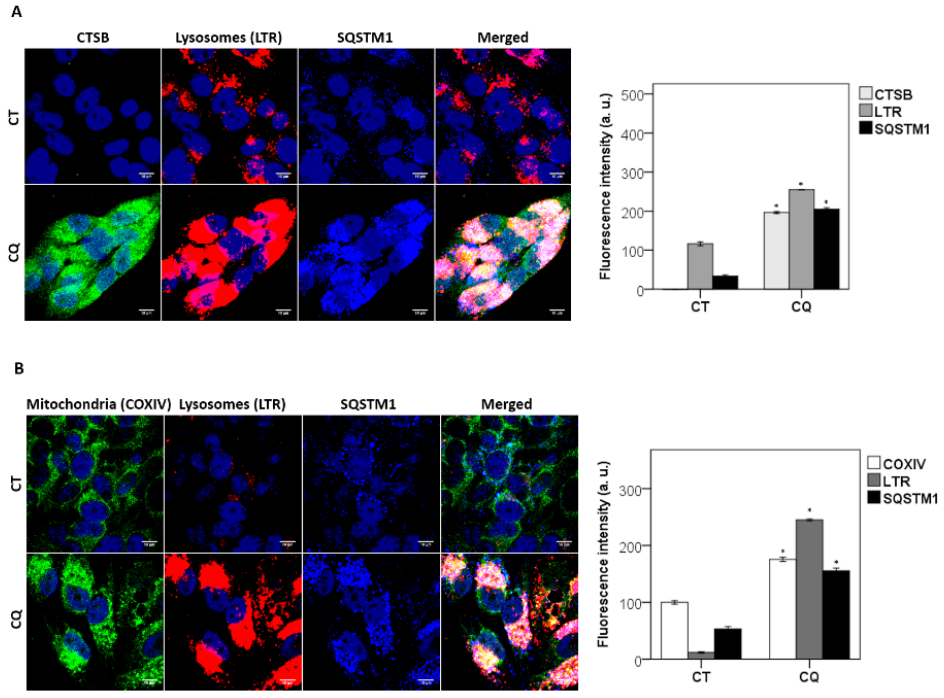

Figure 3: The effects of CQ-treatment are also related to autophagy inhibition in the malignant cell (HeLa). **(A)** At T2 fluorescence images of non-treated (CT) and treated HeLa cells with CQ (60 µM) stained for CTSB (green fluorescence), LysoTracker™ red DND-99 (red fluorescence) and SQSTM1 (blue fluorescence). Bars represent the mean fluorescence intensity considering independent cells. **(B)** At T2 fluorescence micrographs of non-treated (CT) and treated HeLa cells with CQ (60 µM) followed by immunostaining for COXIV (green fluorescence) and SQSTM1 (blue fluorescence). Bars correspond to the mean fluorescence intensity of COXIV and SQSTM1. T1 = 0 h; T2 = 24 h after CQ treatment. We obtained all results from at least three independent experiments and expressed as mean values ± standard error. We indicated the significance levels as $^{*}p<0.0001$. Scale bars: 10 µm.

At long-term response, CQ can trigger senescence

Some reports have shownthe potential relationship between autophagy and senescence in cancer cells exposed to chemotherapeutics agents (e.g., doxorubicin and camptothecin) [38],andinnonmalignantcells exposed to pentacyclic triterpenoid betulinicacid[15]. Thus,we analyzed whether the LC3B-II profile was associated with an increase of nuclei abnormality at T3 in both nonmalignant HaCaT and human carcinoma HeLa cells (Figure 4A). Cells treated with CQ exhibited a remarkable alteration in a nuclear morphometric pattern associated with LC3B-II accumulation in comparison to control (Figures 4A). Note that these abnormalities were evident in both nonmalignant and in tumor cells (Figure 4A, traced line, and Figure 4B). To confirm if the dysfunctional autophagy induced by CQ treatment would end up in senescence, we quantified the nuclear alterations using Nuclear Morphometric Analysis (NMA) [25]. According to Nuclear Irregularity Index (NII), at T3 after CQ (60 µM), we observed nuclear morphological features (i.e., large and regular, LR) suggestive of senescence [15, 25] both in HaCaT and HeLa. The presence of LR- nuclei significantly increased in treated HaCaT (p=0.006), and HeLa (p=0.014) compared to control (Figure 4B and 4C). Accordingly, in both cell lines, nuclei showed area above the "Normal ellipse N," but with NII like control (upper right squares, Figure 4C). Interestingly, these morphological nuclei alterations were observed in HaCaT cells positive for the senescence-associated beta-galactosidase (SA-βgal) biomarker after CQ treatment (Figure 4D), which indicates a typical senescence phenotype[39].

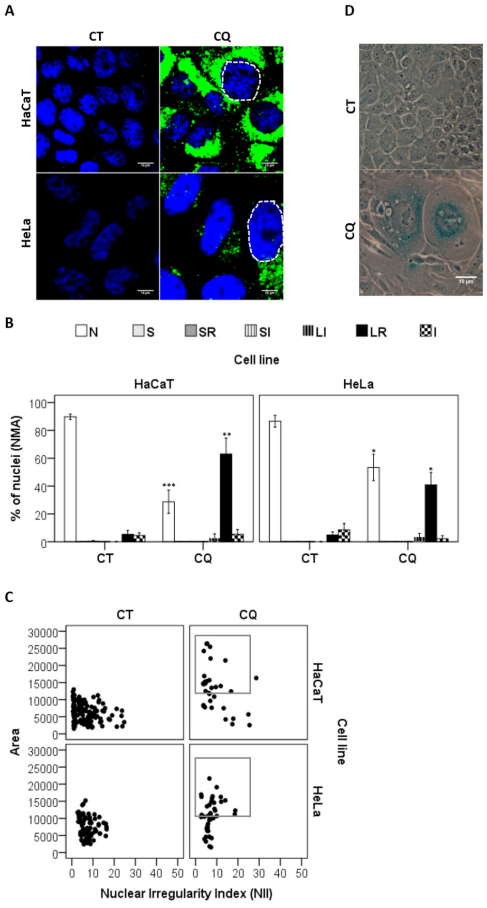

Figure 4: Impact of autophagy inhibition on CQ-induced senescence in nonmalignant HaCaT and carcinoma HeLa cells. **(A)** At T3 images of non-treated (CT) and treated cells with CQ (60 µM) and immunostaining for LC3B-II. **(B)** T3 after treatment with CQ (60 µM), we applied nuclear morphometric analysis (NMA for analyzing area and irregularities of nuclei. N = Normal nuclei; S = Small nuclei; SR = Small/regular nuclei; SI = Small/irregular nuclei; LI = Large/irregular nuclei; LR = Large/regular nuclei; I = Irregular nuclei. **(C)** Representative scatter-plots of control and CQ-treated cells showing nuclear morphometric parameters - area and Nuclear Irregularity Index (NII). **(D)** At T4 cytochemical analysis of SA-β galactosidase activity after CQ (60 µM). Micrographs showed a significant increase in the activity of SA-β galactosidase in HaCaT cells after CQ compared to CT. T3 = 48 h after CQ- treatment for 24 h. Scale bars: 10 µm.

All morphological features mentioned suggest that CQ triggers cell senescence in both human nonmalignant and tumor cells, probably due to autophagy impairment (Figures 2-4). One of the possible outcomes of impaired autophagy is the accumulation of lipofuscin, a nondegradable oxidation product of lipids and proteins commonly found in senescent or aged cells [15, 26, 40–42]. After treatment of HaCaT with CQ (60 µM), we checked for the presence of lipofuscin. Lipofuscin was detected at T3 in CQ-treated cells as electrodense perinuclear granules (see white arrows Figure 5A) within single membrane-vesicles suggestive of autolysosomes (Figure 5A). The perinuclear lipofuscin granules were detected by Fluorescence Lifetime Imaging Microscopy (FLIM), supporting the hypothesis that CQ promoted lipofuscinogenesis as a long-term response in HaCaT (Figure 5B). Note that fluorescence lifetime detected in CQ-treated cells was around 2 ns, a value close to the reported for lipofuscinogenesis upon UVA radiation of HaCaT (1.7 ns) [26]. In summary, HaCaT accumulated lipofuscin upon CQ-treatment, which is indicative of autophagy impairment and senescence [15].

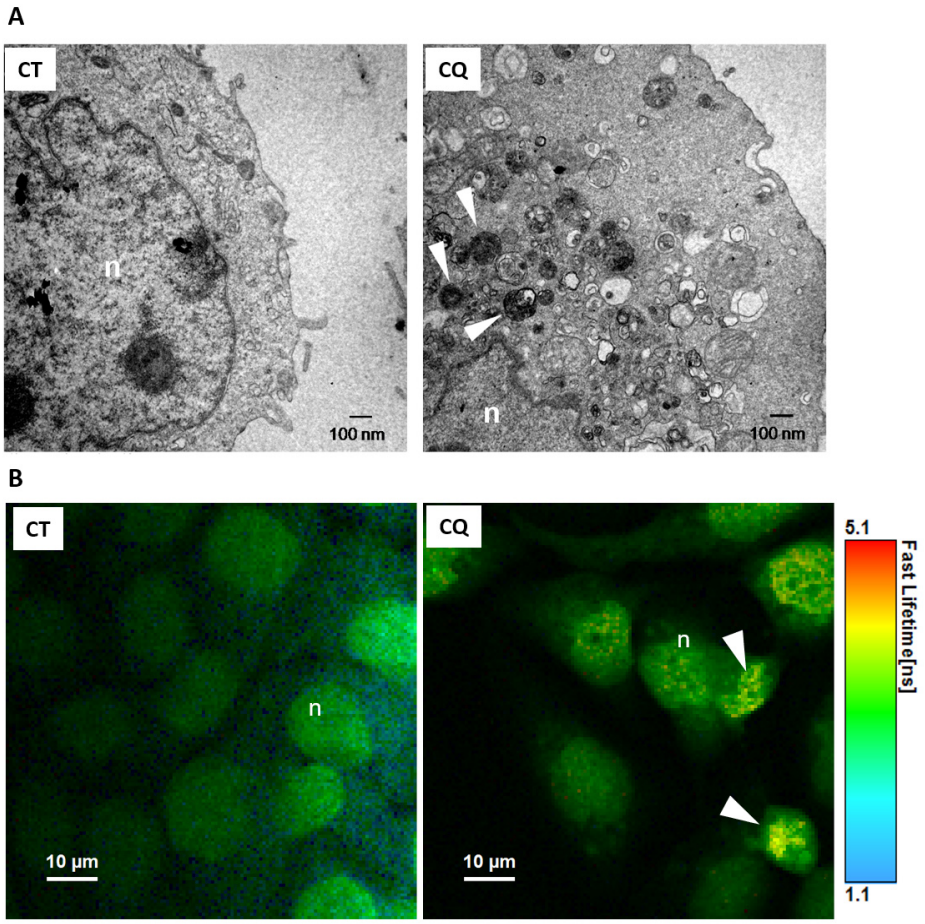

Figure 5: Analysis of lipofuscinogenesis in HaCaT. **(A)** Transmission electron microscopy of non-treated (CT) and treated cells with CQ (60 µM) cells at T3, which showed electrodense granules accumulation (indicated by white arrows) in the perinuclear region, as typically observed for lipofuscin accumulation. n = nucleus. **(B)** Fluorescence Lifetime Imaging Microscopy (FLIM) non-treated (CT) and treated cells with CQ (60 µM) at T3, showing the accumulation of fluorescent granules (white arrows) around the nucleus (n). T1 = after treatment for 24 h; T2 = 24 h after T1. Scale bars: 100 nm (A) or 10 µm (B).

Low CQ dose is enough when associated with mitochondrial injury at the long-term response

We have demonstrated that CQ triggers cell death in nonmalignant cells at concentrations (i.e., 60µM) below the IC50 values reported for several cancer cells (see Table 2). Besides, we have highlighted the importance of evaluating CQ effects on a long-term response instead of a short one in both nonmalignant and malignant cells (see Figures 4 and 5). We then searched for a concentration in which

CQ would selectively kill human tumor cells (Figure 6A). By treating several human tumor cell lines (A549, HT29, HepG2, MCF7, SKMEL-25, and SKMEL-28) with CQ at 3-fold lower concentration (i.e., 20 µM), we provided a systematic and comparative analysis of its cytotoxic profile at T3 (Figure 6A). Noteworthy, HaCaT remained viable, probably due to a more efficient autophagy rescue (Figure 1A). The human colon carcinoma cell (HT29) was the most susceptible, followed by the cutaneous melanoma (SKMEL-25), lung (A549), and liver (HepG2) carcinoma cells (Figure 6A).

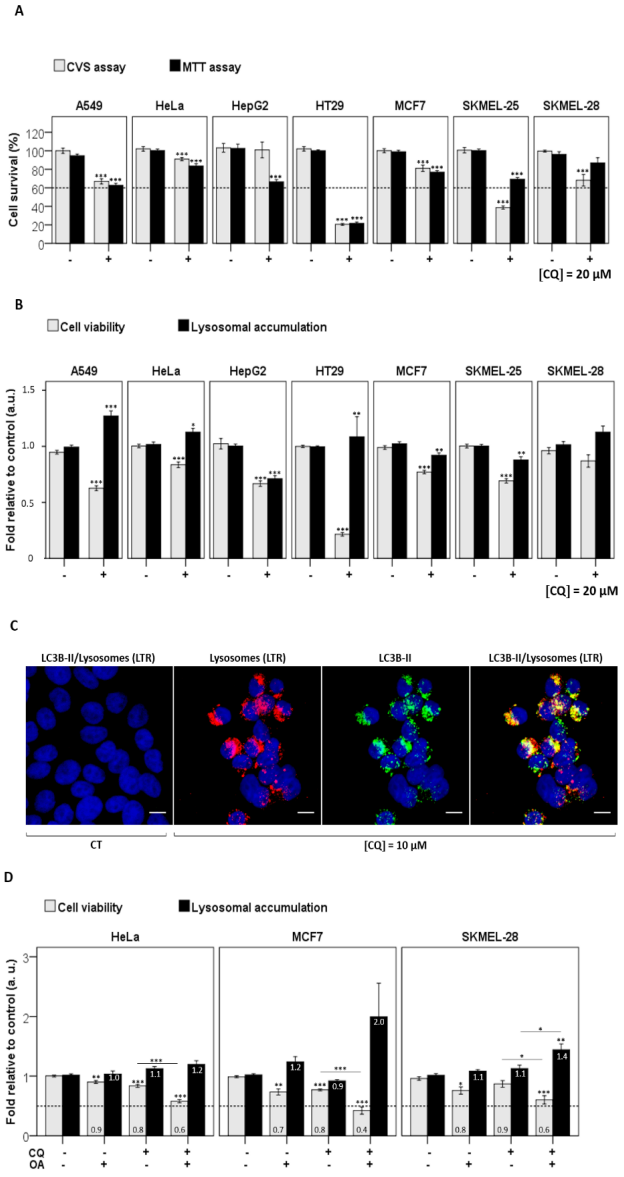

Figure 6: CQ effects on human tumor cells (HeLa, HT29, HepG2, MCF7, SKMEL- 25, and SKMEL-28). **(A)** T3 after treatment with CQ (20 µM), the cell survival determined by CVS and MTT. **(B)** At the same condition in A, MTT response was associated with lysosomal levels by AAU. **(C)** T3 after treatment with CQ (10 µM) fluorescence images of HT29 showed DAPI-stained nucleus, green LC3B-II immunoassay, and red lysosomes stained, indicating autolysosomes formation. **(D)** CQ effects on HeLa, MCF7, and SKMEL-28 cells with regards to mitochondrial damage after treatment with the pentacyclic triterpenoid oleanolic acid (OA). At T3 MTT response of treated cells in the absence (-) or presence (+) of CQ (20 µM) and, or OA (20 µM), was associated with lysosomal levels by AAU. T1 = 0 h; T3 = 48 h after CQ-treatment during 24 h. We obtained all results from at least three independent experiments and expressed as mean values ± standard error. We indicated the significance levels as $^{*}p<0.05$, $^{**}p<0.01$ and $^{***}p<0.001$. Scale bars: 10 µm.

To investigate whether this decrease in cell survival was intrinsically associated with lysosomal accumulation, we applied the AAU platform [13]. Indeed, the cell survival significantly decreased as lysosomal mass increased in both A549 and HT29 (Figure 6B), suggesting activation of autophagy-associated cell death as previously reported for other modulators/inhibitors of autophagy [13,15,20,21,35]. To confirm if lysosomal accumulation shown in Figure 6B corresponded to autolysosomes, we performed a double-staining for LC3B-II and lysosomes (LTR) in HT29 cells at T3 (Figure 6C). We noted a remarkable increase of LC3B-II co-localized with more abundant lysosomes even at a 6-fold lower CQ concentration (i.e., 10 µM), indicating the accumulation of non-functional autolysosomes, a hallmark of RCD by autophagy [19,20,36].

Interestingly, a combined treatment with CQ and the pentacyclic triterpenoid Oleanolic Acid (OA) significantly increased the toxicity of cancer cells (Figure 6D). Upon this condition, the cell death associated with lysosomal accumulation dramatically increased for all CQ-resistant cells HeLa, MCF7, and SKMEL-28 (Figure 6A). OA significantly reduced the mitochondrial membrane potential (ΔΨm) as quantified by MitoTracker™ orange CMTMRos in MCF7 cells (Figure 7A). By promoting parallel damage in mitochondria (OA) and lysosomes (CQ), we sensitized the caspase-3 deficient cell (MCF7) to autophagy-associated cell death (Figure 6D). Accordingly, there was a remarkable accumulation of LC3B-II and autolysosomes in MCF7 cells after the combined CQ-OA treatment (Figure 7B).

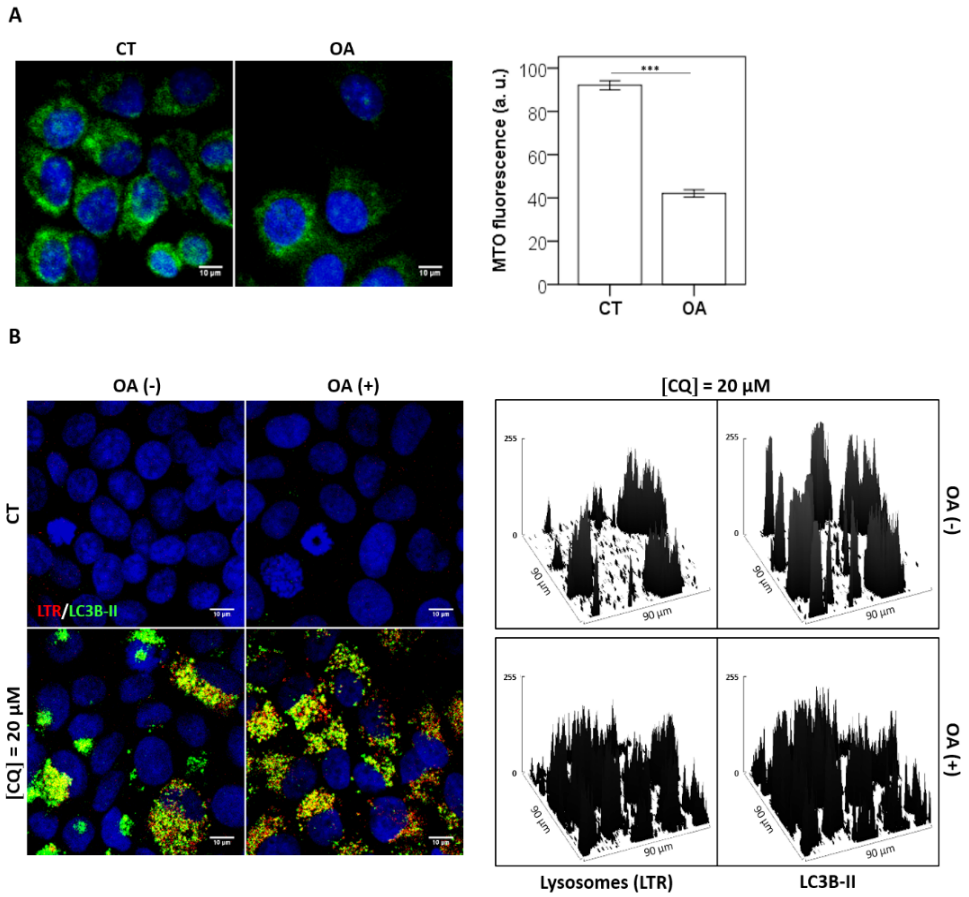

Figure 7: CQ effects on MCF7 breast adenocarcinoma cells regarding mitochondrial damage after treatment with the pentacyclic triterpenoid Oleanolic Acid (OA). **(A)** Following staining with MitoTracker™ orange CMTMRos (50 nM), we monitor mitochondrial inner transmembrane potential (ΔΨm) after OA-treatment (20 µM) for 3 h. **(B)** Confocal microscopy of non-treated (CT) and treated cells with CQ (20 µM) and, or OA (20 µM) at T3. Fluorescence images of MCF7 showed DAPI-stained nucleus, green LC3B-II immunoassay, and red lysosomes stained, indicating autolysosomes formation. Surface plots show the fluorescence intensity of lysosomes (LTR) and LC3B-II. T1 = 0 h and T3 = 48 h after incubation with CQ during 24 h. Scale bars: 10 µm.

Discussion

Our findings differed significantly from those reported in the literature (Table 2), probably due to the long period of evaluation (i.e., 48 h or 96 h) after CQ treatment for 24 h. Also, we found that CQ, even at a lower non-cytotoxic dose (20 μM) for nonmalignant HaCaT cells, could trigger autophagy-associated cell death in tumor cells, mainly when associated with the triterpenoid compound. It occurs due to increased cellular stress caused by non-functional lysosomes after CQ incapable of digesting damaged mitochondria by OA. Therefore, the sensitization of tumor cells to CQ upon treatment with the pentacyclic triterpenoid OA relies on the parallel damage in mitochondria and lysosomes that can significantly increase CQ cytotoxicity in apoptosis-resistant MCF7 breast adenocarcinoma cells [43]. Mainly, autophagy activated by OA is switched to negative outcomes with the promotion of autophagy-associated cell death when occurred parallel damage in lysosomes by CQ [20]. We believe that this concept will help the development of new drugs against aggressive cancers.

The concept of late CQ cytotoxicity relies on the lysosomal impairment that dictates a lysosomal-mitochondrial axis of stress that culminates in autophagy-associated cell death, lipofuscinogenesis, nuclei abnormalities, and the promotion of the senescence-associated beta-galactosidase hallmark of aging or senescence [14,15,39]. Importantly, the CQ-induced lipofuscin may act as a potent visible-light photosensitizer, generating premutagenic lesions in nuclear DNA, reduction of the efficacy of the lysosomal and antioxidant systems that results in lipid peroxidation, protein oxidation and inhibition of the proteasomal activity [26,44-46]. In this context, our findings on long term treatment indicate that CQ can be a "double-edged sword," being therapeutically useful and potentially harmful for cells.

Taking together CQ exhibits toxicity in a time-dependent manner since it is associated with autophagy inhibition that reduces the proliferation of cells, also triggering senescence and aging. Most reports explain CQ biological effects because of unprotonated form that across the lysosomal membranes and become protonated and trapped inside lysosomes [2]. However, we speculate that a high concentration of CQ in lysosomal lumen disturbs the binding of Lysosomal Enzymes (LE) to the inner lysosomal membrane, which results in lysosomal enzymes detachment [47]. Thus, like cationic amphiphilic agents like desipramine and chlorpromazine, CQ probably inhibits lysosomal enzymes, including acid sphingomyelinase, acid ceramidase, and phospholipase A, C, and D, despite not disturbing the activity of cathepsins (B and L) [48-51]. Although activities of cathepsins B and L significantly increased upon CQ, they were not capable of digesting lysosomal cargo (e. g. mitochondria), leading to autophagy-associated cell death. Noteworthy, this property has rendered CQ the most widely used drug to inhibit autophagy *in vitro* and *in vivo* [2,6], which correlated with its pharmacophoric action as anti-malarial, anti-inflammatory as well as anti-tumor drug.

Conclusion

Our data demonstrate that CQ causes harmful effects on tumor cells (SKMEL- 25, SKMEL-28, HeLa, HT29, HepG2, and MCF7), which is related to lysosomal accumulation and autophagy inhibition. We showed the CQ harmful effects ended up higher in a long term-response compared to shorter ones. Moreover, low CQ concentration (i.e., 20 μM) is enough to reduce cell proliferation when associated with the triterpenoid OA. Our work provided insights into the promising role of CQ as an antitumor drug, mainly when we considered lower doses and its late effects.

Acknowledgments

The authors are grateful to Alessandra Araújo de Sousa, Ana C. Viotto, Ingrid Torres Lima, Luana de Souza Barbosa, Laryssa Santos, and Larissa N. Xavier de Albuquerque for technical assistance; Adriana Y. Matsukuma and Wilton J. R. Lima for helping in confocal microscopy and flow cytometry. This work was supported by FAPESP (Fundação de Amparo à Pesquisa do Estado de São Paulo) [grant numbers 12/50680-5, 13/07937-8, 13/16532-1, 16/24435-4, 16/07642-6 and 18/22922-0]; CNPq (Conselho Nacional de Desenvolvimento Científico e Tecnológico) and PNPD (Programa Nacional de Pós Doutorado)/CAPES (Coordenação de Aperfeiçoamento de Pessoal de Nível Superior)/ FINEP (Financiadora de Estudos e Projetos) [grant number 02533/09-0] and CAPES finance code 001.

References

1. Breckenridge AM, Winstanley PA (1997) Clinical pharmacology and malaria. Annals of tropical medicine and parasitology 91: 727-733.
2. Solomon VR, Lee H (2009) Chloroquine and its analogs: A new promise of an old drug for effective and safe cancer therapies. European Journal of Pharmacology 625: 220-233.
3. Wiesner J, Ortmann R, Jomaa H, Schlitzer M (2003) New Antimalarial Drugs. Angewandte Chemie - International Edition 42: 5274-5293.
4. Vazquez-Martin A, López-Bonetc E, Cufí S, Oliveras-Ferraros C, Del Barco S, et al. (2011). Repositioning chloroquine and metformin to eliminate cancer stem cell traits in pre-malignant lesions. Drug Resistance Updates 14: 212-223.
5. White E (2015) The role for autophagy in cancer. Journal of Clinical Investigation 125: 42-46.
6. Kimura T, Takabatake Y, Takahashi A, Isaka Y (2013) Chloroquine in cancer therapy: A double-edged sword of autophagy. Cancer Research 73: 3-7.
7. Mauthe M, Orhon I, Rocchi C, Zhou X, Luhr M, et al. (2018) Chloroquine inhibits autophagic flux by decreasing autophagosome-lysosome fusion. Autophagy.

8. Mizushima N, Levine B, Cuervo AM, Klionsky DJ (2008) Autophagy fights disease through cellular self-digestion. Nature: 451.

9. Aymard E, Barruche V, Naves T, Bordes S, Closs B, et al. (2011) Autophagy in human keratinocytes: an early step of the differentiation? Experimental dermatology 20: 263-268.

10. Salminen A, Kaarniranta K (2009) Regulation of the aging process by autophagy. Trends in molecular medicine 15: 217-224.

11. Cuervo AM, Bergamini E, Brunk UT, Dröge W, Ffrench M, et al. (2005) Autophagy and aging: the importance of maintaining "clean" cells. Autophagy 1: 131-140.

12. Rubinsztein DC, Mariño G, Kroemer G (2011) Autophagy and aging. Cell 146: 682-695.

13. Martins WK, Severino D, Souza C, Stolf BS, Baptista MS (2013) Rapid screening of potential autophagic inductor agents using mammalian cell lines. Biotechnology Journal 8: 730-737.

14. Brunk UT, Terman A (2002) The mitochondrial-lysosomal axis theory of aging: Accumulation of damaged mitochondria as a result of imperfect autophagocytosis. European Journal of Biochemistry 269: 1996-2002.

15. Martins WK, Gomide AB, Costa ÉT, Junqueira HC, Stolf BS, et al. (2017) Membrane damage by betulinic acid provides insights into cellular aging. Biochimica et Biophysica Acta (BBA) - General Subjects 1861: 3129-3143.

16. Boukamp P, Petrussevska RT, Breitkreutz D, Hornung J, Markham A, et al. (1988) Normal keratinization in a spontaneously immortalized aneuploid human keratinocyte cell line. The Journal of cell biology 106: 761-71.

17. Carey TE, Takahashi T, Resnick L, Oettgen HF, Old LJ (1976) Cell surface antigens of human malignant melanoma: mixed hemadsorption assays for humoral immunity to cultured autologous melanoma cells. Proceedings of the National Academy of Sciences of the United States of America 73: 3278-3282.

18. Scherer WF, Syverton JT, Gey, GO (1953) Studies on the propagation in vitro of poliomyelitis viruses. IV. Viral multiplication in a stable strain of human malignant epithelial cells (strain HeLa) derived from an epidermoid carcinoma of the cervix. The Journal of experimental medicine 97: 695- 710.

19. Klionsky DJ, Abdelmohsen K, Abe A, Abedin MJ, Abeliovich H, et al. (2016) Guidelines for the use and interpretation of assays for monitoring autophagy (3rd edition). Autophagy 12: 1-222.

20. Martins WK, Costa ÉT, Cruz MC, Stolf BS, Miotto R, et al. (2015) Parallel damage in mitochondrial and lysosomal compartments promotes efficient cell death with autophagy: The case of the pentacyclic triterpenoids. Scientific Reports 5: 12425.

21. Martins WK, Santos NF, Rocha C. de S, Bacellar IOL, Tsubone TM, et al. (2019) Parallel damage in mitochondria and lysosomes is an efficient way to photoinduce cell death. Autophagy 15: 259-279.

22. Robbins E, Marcus, PI (1963) Dynamics of Acridine Orange-Cell Interaction. I. Interrelationships of Acridine Orange Particles and Cytoplasmic Reddening. The Journal of cell biology 18: 237-250.

23. Terman A, Kurz T (2013) Lysosomal iron, iron chelation, and cell death. Antioxidants & redox signaling, 18: 888-898.

24. Bolte S, Cordelières FP (2006) A guided tour into subcellular colocalization analysis in light microscopy. Journal of microscopy 224: 213-232.

25. Filippi-Chiela EC, Oliveira MM, Jurkovski B, Callegari-Jacques SM, da Silva VD, et al. (2012) Nuclear morphometric analysis (NMA): screening of senescence, apoptosis and nuclear irregularities. PloS one 7: e42522.

26. Tonolli PN, Chiarelli-Neto O, Santacruz-Perez C, Junqueira HC, Watanabe IS, et al. (2017) Lipofuscin Generated by UVA Turns Keratinocytes Photosensitive to Visible Light. Journal of Investigative Dermatology 137: 2447-2450.

27. Dimri GP, Lee XH, Basile G, Acosta M, Scott C, et al. (1995) A Biomarker That Identifies Senescent Human-Cells in Culture and in Aging Skin in-Vivo. Proceedings of the National Academy of Sciences of the United States of America 92: 9363-9367.

28. Geng Y, Kohli L, Klocke BJ, Roth KA (2010) Chloroquine-induced autophagic vacuole accumulation and cell death in glioma cells is p53 independent. Neuro-oncology 12: 473-481.

29. Verschooten L, Barrette K, van Kelst S, Rubio Romero N, Proby C, et al. (2012) Autophagy Inhibitor Chloroquine Enhanced the Cell Death Inducing Effect of the Flavonoid Luteolin in Metastatic Squamous Cell Carcinoma Cells. PLoS ONE 7: 1-11.

30. Schonewolf C, Mehta M, Schiff D, Wu H, Haffty BG, et al. (2014) Autophagy inhibition by chloroquine sensitizes HT-29 colorectal cancer cells to concurrent chemoradiation. World journal of gastrointestinal oncology 6: 74-82.

31. Verbaanderd C, Maes H, Schaaf MB, Sukhatme VP, Pantziarka P, et al. (2017) Repurposing drugs in oncology (ReDO) - Chloroquine and hydroxychloroquine as anti-cancer agents. Ecancermedicalscience 11: 1-35.

32. Boya P, Kroemer G (2008) Lysosomal membrane permeabilization in cell death. Oncogene 27: 6434-6451.

33. Repnik U, Hafner Česen M, Turk B, (2014) Lysosomal membrane permeabilization in cell death: concepts and challenges. Mitochondrion 19: 49-57.

34. Martins WK, Santos NF, Rocha C.de S, Bacellar IOL, Tsubone TM, et al. (2019) Parallel damage in mitochondria and lysosomes is an efficient way to photoinduce cell death. Autophagy 15: 259-279.

35. Tsubone TM, Martins WK, Pavani C, Junqueira HC, Itri R, et al. (2017) Enhanced efficiency of cell death by lysosome-specific photodamage. Scientific Reports 7: 6734.

36. Galluzzi L, Baehrecke EH, Ballabio A, Boya P, Bravo□San Pedro JM, et al. (2017) Molecular definitions of autophagy and related processes. The EMBO Journal 36: 1811-1836.

37. Lemasters JJ (2014) Variants of mitochondrial autophagy: Types 1 and 2 mitophagy and micromitophagy (Type 3). Redox Biology. Elsevier.

38. Goehe RW, Di X, Sharma K, Bristol ML, Henderson SC, et al. (2012) The Autophagy-Senescence Connection in Chemotherapy: Must Tumor Cells (Self) Eat Before They Sleep? Journal of Pharmacology and Experimental Therapeutics 343: 763-778.

39. Salama R, Sadaie M, Hoare M, Narita M (2014) Cellular senescence and its effector programs. Genes & development 28: 99-114.

40. Salmonowicz H, Passos JF (2017) Detecting senescence: a new method for an old pigment. Aging Cell 16: 432-434.

41. Terman A, Dalen H, Eaton JW, Neuzil J, Brunk UT (2004) Aging of cardiac myocytes in culture: Oxidative stress, lipofuscin accumulation, and mitochondrial turnover. In Annals of the New York Academy of Sciences 1019: 70-77.

42. Wang CHH, Wu SBB, Wu YTT, Wei YHH (2013) Oxidative stress response elicited by mitochondrial dysfunction: Implication in the pathophysiology of aging. Experimental Biology and Medicine 238: 450- 460.

43. dos Santos AF, Terra LF, Wailemann RAM, Oliveira TC, Gomes V.de M, et al. (2017) Methylene blue photodynamic therapy induces selective and massive cell death in human breast cancer cells. BMC Cancer 17: 194.

44. Höhn A, Jung T, Grimm S, Grune T (2010) Lipofuscin-bound iron is a major intracellular source of oxidants: Role in senescent cells. Free Radical Biology and Medicine 48: 1100-1108.

45. Shamsi FA, Boulton M (2018) Inhibition of RPE Lysosomal and Antioxidant Activity by the Age Pigment Lipofuscin.

46. Davies S, Elliott MH, Floor E, Truscott TG, Zareba M, Sarna T, et al. (2001) Photocytotoxicity of lipofuscin in human retinal pigment epithelial cells. Free radical biology & medicine 31: 256-265.

47. Kornhuber J, Tripal P, Reichel M, Terfloth L, Bleich S, et al. (2008) Identification of new functional inhibitors of acid sphingomyelinase using a structure-property-activity relation model. Journal of Medicinal Chemistry 51: 219-237.

48. Elojeimy S, Holman DH, Liu X, El-Zawahry A, Villani M, et al. (2006) New insights on the use of desipramine as an inhibitor for acid ceramidase. FEBS Letters 580: 4751-4756.

49. Jaffrézou JP, Chen G, Durán GE, Muller C, Bordier C, et al. (1995) Inhibition of lysosomal acid sphingomyelinase by agents which reverse multidrug resistance. Biochimica et biophysica acta 1266: 1-8.

50. Matsuzawa Y, Hostetler KY (1980) Inhibition of lysosomal phospholipase A and phospholipase C by chloroquine and 4,4'-bis(diethylaminoethoxy) alpha, beta-diethyldiphenylethane. Journal of Biological Chemistry 255: 5190-5194.

51. Chi KH, Wang YS, Huang YC, Chiang HC, Chi MS, et al. (2016) Simultaneous activation and inhibition of autophagy sensitizes cancer cells to chemotherapy. Oncotarget 7: 58075-58088.

52. Martinez-Outschoorn UE, Pavlides S, Whitaker-Menezes D, Daumer KM, Milliman JN, et al. (2010) Tumor cells induce the cancer associated fibroblast phenotype via caveolin-1 degradation: Implications for breast cancer and DCIS therapy with autophagy inhibitors. Cell Cycle 9: 2423-2433.

53. Molenaar RJ, Coelen RJS, Khurshed M, Roos E, Caan MWA, et al. (2017) Study protocol of a phase IB/II clinical trial of metformin and chloroquine in patients with IDH1-mutated or IDH2- mutated solid tumours. BMJ Open 7: 1-12.

54. Briceño E, Reyes S, Sotelo J (2003) Therapy of glioblastoma multiforme improved by the antimutagenic chloroquine. Neurosurgical focus 14: e3.

55. Sotelo J, Briceño E, López-González MA (2006) Adding chloroquine to conventional treatment for glioblastoma multiforme: a randomized, double- blind, placebo-controlled trial. Annals of internal medicine 144: 337-343.

56. Durie BGM, Harousseau JL, Miguel JS, Bladé J, Barlogie B, et al. (2006) International Myeloma Working Group. International uniform response criteria for multiple myeloma. Leukemia 20: 1467-1473.

57. Abdel-Aziz AK, Shouman S, El-Demerdash E, Elgendy M, Abdel-Naim B (2014) Chloroquine synergizes sunitinib cytotoxicity via modulating autophagic, apoptotic and angiogenic machineries. Chemico-Biological Interactions 217: 28-40.

58. Zheng Y, Zhao YL, Deng X, Yang S, Mao Y, et al. (2009) Chloroquine inhibits colon cancer cell growth in vitro and tumor growth in vivo via induction of apoptosis. Cancer Investigation 27: 286-292.

59. Fan C, Wang W, Zhao B, Zhang S, Miao J (2006) Chloroquine inhibits cell growth and induces cell death in A549 lung cancer cells. Bioorganic and Medicinal Chemistry 14: 3218-3222.

60. Jiang P. Du, Zhao YL, Deng XQ, Mao YQ, Shi W, et al. (2010) Antitumor and antimetastatic activities of chloroquine diphosphate in a murine model of breast cancer. Biomedicine and Pharmacotherapy 64: 609-614.

61. Liu F, Shang Y, Chen S (2014) Chloroquine potentiates the anti-cancer effect of lidamycin on non-small cell lung cancer cells in vitro. Acta Pharmacologica Sinica 35: 645-652.

62. Lin YC, Lin JF, Wen SI, Yang SC, Tsai TF, et al. (2017) Chloroquine and hydroxychloroquine inhibit bladder cancer cell growth by targeting basal autophagy and enhancing apoptosis. Kaohsiung Journal of Medical Sciences 33: 215-223.

63. Fu Z, Xi C, Kuang J, Feng H, Chen L, Liang J, et al. (2018) CQ sensitizes human pancreatic cancer cells to gemcitabine through the lysosomal apoptotic pathway via reactive oxygen species. Molecular Oncology 12: 529-544.

64. Chen PM, Gombart ZJ, Chen JW (2011) Chloroquine treatment of ARPE-19 cells leads to lysosome dilation and intracellular lipid accumulation: possible implications of lysosomal dysfunction in macular degeneration. Cell & Bioscience 1: 10.

65. Divac Rankov A, Ljujić M, Petrić M, Radojković D, Pešić M, et al. (2017) Targeting autophagy to modulate cell survival: a comparative analysis in cancer, normal and embryonic cells. Histochemistry and Cell Biology 148: 529-544.